Implementation of a Transformerless Common-Mode Active Filter for Offline Converter Systems

Marcelo Lobo Heldwein, *Member, IEEE*, Hans Ertl, *Member, IEEE*,
Juergen Biela, *Member, IEEE*, and Johann W. Kolar, *Senior Member, IEEE*

***Abstract*—This paper presents a study and practical implementation of an active filter employing a high-frequency (HF) power amplifier and passive-filter components to be connected to the ac power lines in order to mitigate common-mode conducted emissions of three-phase pulsewidth modulation converter systems. The filter topology is chosen from different possibilities listed in a literature survey and studied regarding practical implementation issues, where requirements for an HF power amplifier to be applied in active filtering are derived. Special attention is put on the stability analysis where the challenges for the feedback are discussed, and a simple feedback structure is proposed. Other feedback concepts are analyzed, and limitations posed by stability requirements are presented. A prototype is designed and built, from which mathematical and experimental results are obtained demonstrating the potential and limitations of such a system.**

***Index Terms*—Active filter, conducted emissions, three-phase filters, three-phase PWM converters.**

I. Introduction

In MODERN power-electronic systems, volumetric densities typically range between 1 and 3 kW/dm^3, depending on the employed technology and switching frequency. For higher power densities, higher switching frequencies can be used, but the electromagnetic compatibility (EMC) filtering components [1] still occupy a large volume in the system, more than 30% in some cases. In a world where system and application space is becoming more and more expensive, the volumetric reduction of power-supply components is of great importance. A proposed solution for the size reduction of EMC filters is the use of active systems [2]–[6], commonly called active filters, instead of fully passive filters. High-frequency (HF) active filters are broadly employed in signal processing, where low current and voltage levels are present. However, as power levels increase, the construction of such systems becomes critical. Since wideband amplifiers are to be used, these should be able to handle high current and voltage levels. This challenge motivates research in this field and is addressed in the following.

The scope of this work is limited to the common-mode (CM) conducted emissions mainly in the frequency range from 150 kHz to 30 MHz. The connection from the EMC filter to the power circuits is on the ac mains side where a large 50- or 60-Hz frequency component is present, along with its low-frequency harmonic contents. In this application, the main function of the filter is the reduction of HF CM emissions. For that, the filters are based on linear HF power amplifiers as switched circuits currently do not provide the required operating bandwidth. The reduction of CM emissions is an important issue in all fields of electronics applications, and the traditional approach is the use of Y-rated capacitors connected from the lines to protective earth (PE) in addition to CM inductors. In most applications, the size of these capacitors is limited due to safety regulations restricting the earth leakage currents, resulting in higher values of the CM filter inductors and larger filter volume, particularly for high-power systems. Aiming for the reduction of the total filter volume while keeping low values of the low-frequency leakage currents, an active circuit, which shapes the frequency response of a capacitor effectively increasing its value for high frequencies, is the solution presented in this paper.

A practical active filter should be able to meet all relevant safety and EMC regulations, as well as high-voltage surge requirements, and the filter stability should be independent from the impedances the filter is connected to. Cost is also a limiting factor, and the active filter should not be more expensive than a conventional passive one.

From the potential advantages of the use of active-filter circuits for reducing high-frequency conducted emissions in power-electronic circuits, the knowledge about the different possible structures and the design of the active EMC filter are essential. Four main types of circuits [3] are cited in the literature and shown in Fig. 1 as simplified single-phase equivalent circuits. The classification into four circuits is based on the types of parameters employed in sensing and actuation paths. The basic strategies rely on the sensing of either current (Fig. 1(a), [4], [5], [7] and Fig. 1(b), [8]–[10]) or voltage (Fig. 1(c), [11]–[13] and Fig. 1(d), [14]–[17]), and in the injection of a shunt current [Fig. 1(b) and (d)] or a series voltage [Fig. 1(a) and (c)] to the ac lines. In addition to the topologies of Fig. 1, other active-filter structures using a combination of the shown circuits can be implemented [18]–[21]. One option is to use a current-sensing feedback in combination with a voltage-sensing feedforward. Other options are to place the active-filter power amplifier at the converter output or at the dc-link

Manuscript received October 13, 2008; revised August 31, 2009. First published September 22, 2009; current version published April 14, 2010.

M. L. Heldwein is with the Power Electronics Institute (INEP), Federal University of Santa Catarina (UFSC), Florianópolis 88040-970, Brazil (e-mail: heldwein@inep.ufsc.br).

H. Ertl is with the Institute of Electrical Drives and Machines, Vienna University of Technology (TUW), 1040 Vienna, Austria (e-mail: j.ertl@tuwien.ac.at).

J. Biela and J. W. Kolar are with the Power Electronic Systems Laboratory, Swiss Federal Institute of Technology (ETH Zurich), 8092 Zurich, Switzerland (e-mail: biela@lem.ee.ethz.ch; kolar@lem.ee.ethz.ch).

Color versions of one or more of the figures in this paper are available online at http://ieeexplore.ieee.org.

Digital Object Identifier 10.1109/TIE.2009.2032204

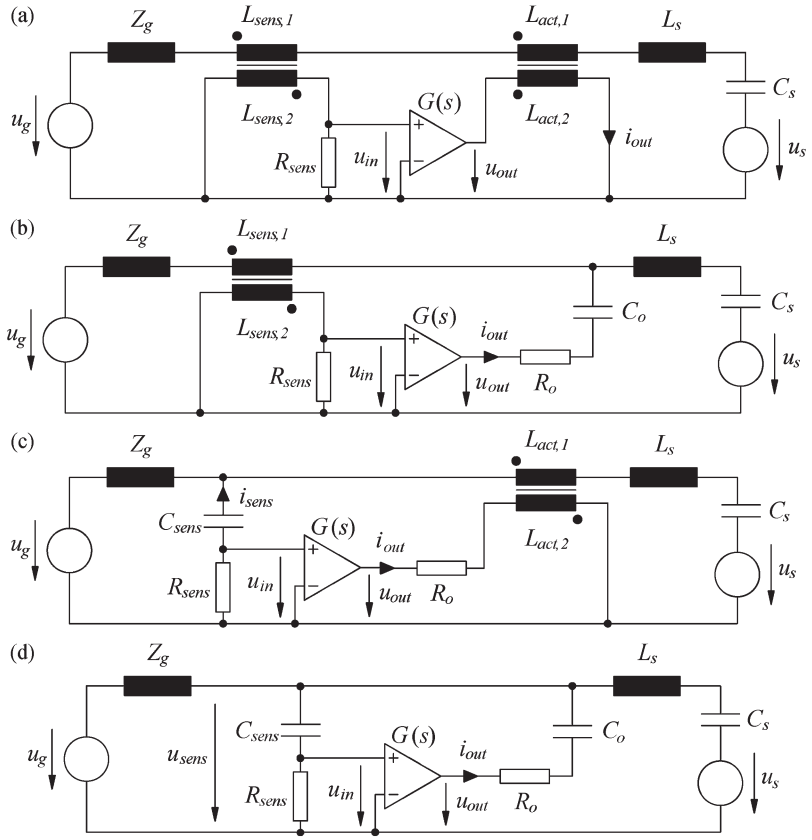

Fig. 1. Basic active-filter structures in their single-phase equivalent circuits. The noise source is modeled as a voltage source in series with a capacitor C_s and an inductor L_s. The mains impedance Z_g is considered inductive. (a) CSVA. (b) CSCA; (c) VSVA. (d) VSCA.

terminals and the sensing devices directly at the ac input lines or even combine two of these [21].

In this paper, a filter topology to be placed directly at the ac lines of a three-phase power system is studied. It comprises a capacitive-coupling actuation and a voltage sensing according to Fig. 1(d) in a single-phase equivalent. The active-filter structure is well known [14]–[17]; therefore, the emphasis is placed on the design of the feedback loop since it determines the system stability and challenges for the practical construction. It is shown that the correct placement of zeros and poles in the feedback path is of high importance [5], [14] for guaranteeing stable operation for a large range of mains and noise-source-impedance conditions. A theoretical basis for the determination of zeros and poles is presented, along with results obtained from a first prototype based on the described theoretical analysis.

II. Selection of Active-Filter Topology and Its Basic Operating Principle

By considering the circuits of Fig. 1, one realizes that the noise-source (C_s and L_s) and the power-grid impedances (Z_g) are usually difficult to predict and/or control [22], [23] but should obviously be included in the stability consideration. For the topologies making use of a line-current-based feedback or actuation employing current transformers, it seems more difficult to decouple the system stability from the source and grid impedances. A difficult issue is that the current transformer needs a large bandwidth, and the simple inclusion of an extra winding in a conventional CM inductor does not always guarantee a good high-frequency magnetic coupling due to construction regarding safety regulations and the poor relative HF permeability characteristics of conventionally used materials. In addition, self-resonances due to the magnetic materials are to be expected as well as winding capacitances degrading the HF properties of the current transformer. The physical dimensions of a current transformer can also represent a drawback of such concepts when compared with capacitive-based ones. For these reasons, the cost of a good HF current transformer must be added to the filtering system. Therefore, a topology based on capacitive sensing of the line voltage and utilizing also capacitors in the actuator stage seems to be a good choice for an active filter connected to the ac lines. The filter topology considered in this work is shown in the simplified schematic in Fig. 2, which corresponds to the circuit in Fig. 1(d).

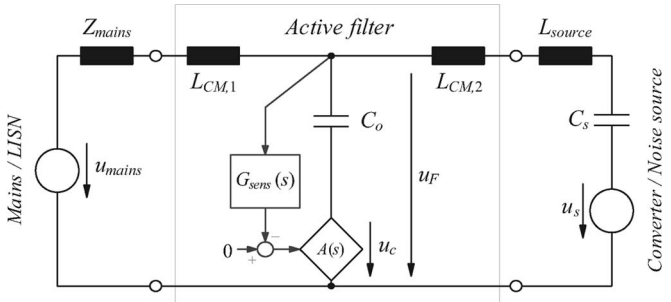

Fig. 2. Simplified single-phase schematic showing the basic principle of the selected CM filtering system.

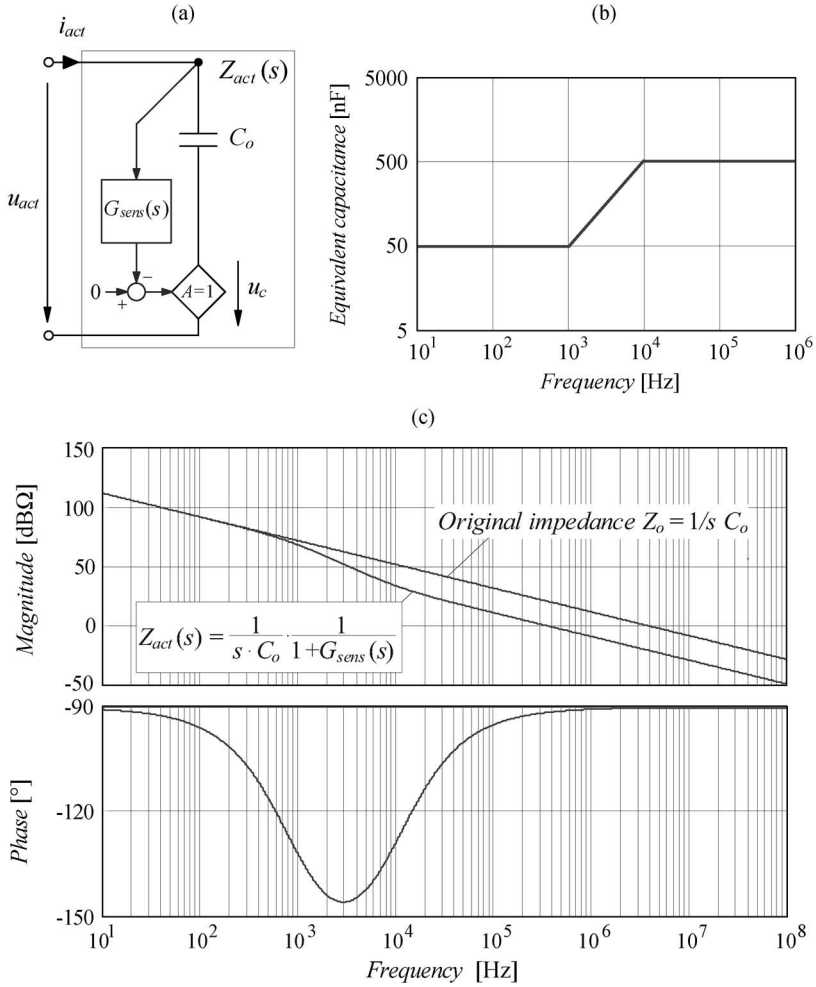

Fig. 3. Basic principle of an active filter with capacitive coupling. (a) Impedance $Z_{\rm act}$ of a capacitor with a voltage-feedback loop. (b) Equivalent capacitance is increased in the higher frequencies through the active-feedback action. (c) Example of impedance curves $Z_{\rm act}(f)$. Illustrating the feedback action.

This topology is composed of two CM inductors ($L_{CM,1}$ and $L_{CM,2}$), one coupling capacitor (C_o), a sensing path ($G_{\rm sens}$) including a low-frequency attenuation network for rejection of any unwanted high-amplitude low-frequency components and an actuator ($A(s)$), which is realized with a linear HF power amplifier ($G_{\rm amp}$), not shown in Fig. 2 due to its interaction with $G_{\rm sens}$ in a practical application. This structure presents some advantages such as the following.

1) The filter structure and its principle are simple, presenting a potentially high stability range, increasing the possible filter attenuation in the frequency band of interest.
2) Both sensing ($G_{\rm sens}$) and output coupling (through C_o) can be performed through Y-rated capacitors;
3) As the needed inductance and capacitance values decrease by the use of an active feedback, better HF performance is achieved than with a nonactive filter, as smaller components usually present higher resonance frequencies [24];
4) The implementation is potentially safe since the feedback sensing is done with low voltages; only a single HF power amplifier needs to be employed.

The use of the topology shown in Fig. 2 has as its main advantage with the use of two CM inductors and a capacitor, which are usually already present in typical CM filters, however, with smaller inductance values. For the case of CM noise filtering, these components are CM chokes and Y-capacitors, which technology are well known and do not make the filter more expensive. Since Y-capacitors have their values limited due to the safety limitation of the allowable earth leakage currents, the main idea with this active-filter topology is to use the existing values of Y-capacitors and virtually increase the capacitance by proper shaping of the feedback-frequency response, thus allowing a noticeable reduction of the inductors, which are usually large, heavy, and costly in high power systems.

The basic principle of the topology shown in Fig. 2 is to increase the equivalent capacitance for high frequencies by using a feedback loop. This is illustrated in Fig. 3 where one can see that, for the lower frequency end, the original capacitance of C_o is effective, but for higher frequencies, an increase in the capacitance is possible as the feedback-gain increases, according to

$$Z_{\rm act}(s) = \frac{U_{\rm act}(s)}{I_{\rm act}(s)} = \frac{1}{sC_o} \cdot \frac{1}{1 + G_{\rm sens}(s)}. \qquad (1)$$

With (1), it can be seen that the capacitance is effectively multiplied by the gain $G_{\rm sens}$. This characteristic is very important in this type of system since the capacitance at low frequency

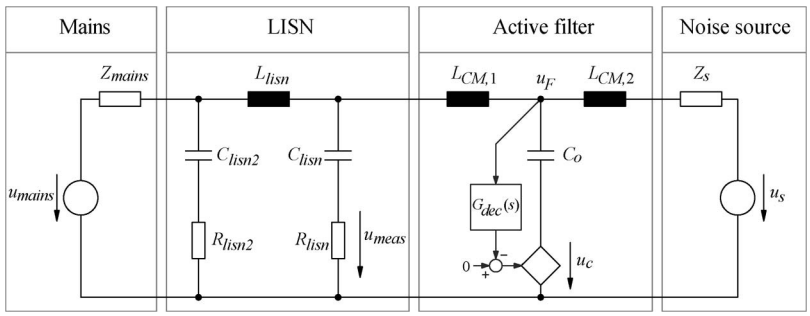

Fig. 4. Single-phase equivalent circuit for the active filter with an LISN included.

should be kept as small as possible due to the limited earth leakage current.

The configuration for the design of the active filter regarding its attenuation is shown in Fig. 4, where the model of a simplified line-impedance stabilization network (LISN) is included. This configuration allows studying of the required filter performance, with R_{lisn}, according to CISPR 16 [25], equal to 50 $\Omega/3$. This is because the three lines of an LISN are in parallel for CM currents.

III. Stability Analysis and Feedback Structure

There are four strict requirements for the filter structure.

1) The attenuation of high frequencies needs to be higher than for a passive filter with the same components.
2) The value of the capacitor (C_o) is limited due to safety considerations (earth leakage currents).
3) The 50/60-Hz and the low-frequency harmonic components present in the voltage u_F are quite large when compared with the high-frequency components. As a requisite, they must be well attenuated in the feedback loop to prevent the amplifier from saturating.
4) The system has to be stable for a large range of noise source and mains impedances.

Once an active part is included in the topology, the natural stability achieved with only the passive elements is not further guaranteed, and a careful study of the stability should be carried out. The study of possible gains in the feedback loop and the sensing/control structures that lead to higher stability margins is of great importance since the 50/60-Hz component requires a high attenuation factor.

The use of Bode diagrams for the stability study is not sensible since the active-filter structures do not fulfill the requirement—steady decrease of the open-loop gain and phase curves [26]—for a straightforward analysis by frequency-domain plots. Thus, the root-locus analysis is the tool to be used.

As a starting point for the stability analysis of the proposed active filter, the circuit shown in Fig. 5 is used, where the reactive components consider the inductive characteristics of the mains and the mainly capacitive nature of the CM noise source. The parasitic elements of the main components, such as the resistances of inductors $L_{CM,1}$ and $L_{CM,2}$, are not explicitly shown, but as it is seen later, they are crucial for the stability analysis.

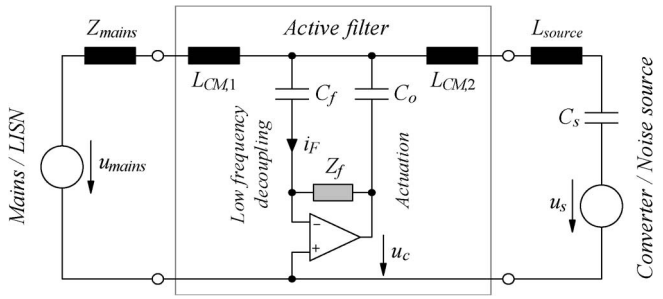

Fig. 5. Basic single-phase equivalent circuit for the active filter including an amplifier and showing the variables of interest (sensing) i_F and (actuation) u_c.

The closed-loop system can have its open-loop transfer function calculated by opening the loop at the output connection of the amplifier u_c. This is a logical step since the output impedance of the amplifier is typically much lower than the input impedance of the output coupling capacitor C_o. By opening the loop, short-circuiting the voltage sources, and assuming that the input voltage of the operational amplifier is zero, a fact that can be assumed because this voltage is much smaller than the voltage across C_f, the system can have its stability analyzed through the circuit shown in Fig. 5, where the impedances $L_{CM,1}$ and Z_{mains} are summed to L_g and the impedances $L_{CM,2}$ and L_{source} to L_s.

The sensing capacitance C_f is also considered since it adds a zero and changes the positions of the poles. With these considerations, the feedback variable of interest is the current i_F, which is multiplied by the impedance Z_f for the final shaping of the feedback loop.

As an example, a Bode plot of the considered plant, for the parameters shown in Fig. 6(a), is shown in Fig. 6(b). The system under consideration is a three-phase adjustable-speed drive (ASD) based on a 6.8-kVA sparse matrix converter (SMC), switching at a frequency of $f_P = 10/20$ kHz (input/output stage switching frequencies). The total capacitance is limited for safety reasons, and the designed value is 22 nF per phase, leading to a total of 66 nF. A decrease of ten times in the former CM filter inductance of around 6 mH is desirable. Therefore, two inductors of 320 μH have been chosen. The noise source may vary depending on the nature of the load (passive, motor), and the minimum value is around 1 nF, which is measured in the SMC without load. The sensing capacitance C_f depends on all the parameters of the complete active circuit, and a value of 14.1 nF is chosen.

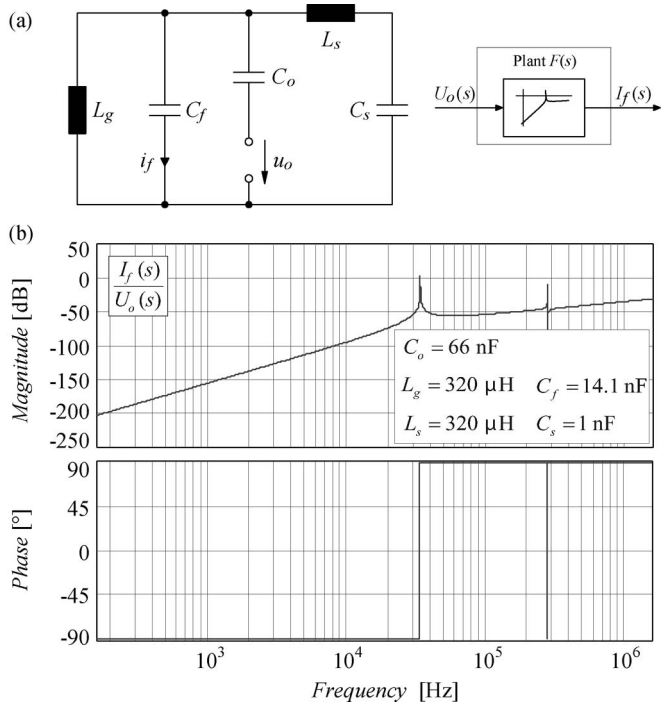

Fig. 6. Circuit used for the stability analysis. (a) The basic circuit of the analyzed active-filter plant with its transfer function. (b) An example of Bode plots for an analyzed active-filter plant.

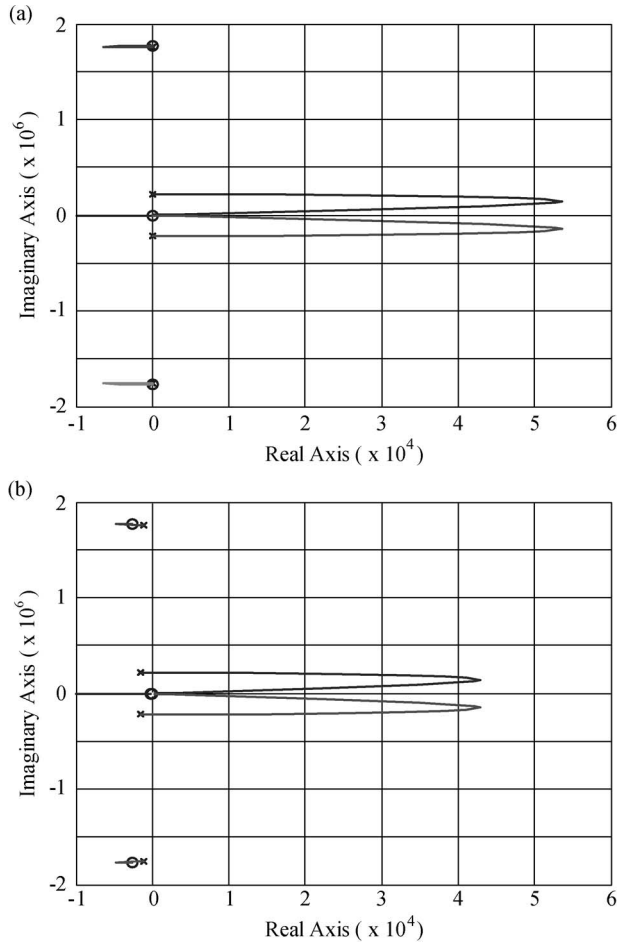

Fig. 7. Root-locus diagrams for the active-filter plant $I_f(s)/U_o(s)$ for the parameters specified in Fig. 6. (a) Root locus for a filter plant purely reactive. (b) Diagram illustrating the changes in the positions of the singularities due to the inclusion of parasitic resistive elements for the same filter plant. The parasitic resistance values are obtained from impedance measurements performed on the filtering components and on the SMC, and the assumed values are shown in the three resistors shown in Fig. 9.

If no damping elements are considered, the root locus for the system of Fig. 5 is plotted in Fig. 7(a) from (2), shown at the bottom of the page.

A proper modeling of the system however requires that the resistive elements of the circuit are considered, as they move the plant singularities to the left half-plane as shown in the root locus of Fig. 7(b). Considering parasitic effects, it is feasible to employ simple feedback structures, which can properly reject the low-frequency components but have their maximum HF gain limited. The analysis of the root-locus plots of Fig. 7 shows that the plant without the inclusion of parasitic resistances would be extremely difficult to stabilize, presenting three zeros at the origin and four poles at the imaginary axis.

As previously cited, a limited supply voltage should be used for the power amplifier, and it is not desirable that the closed-loop system influences the circuit behavior at 50 Hz. For a single-phase system, it is necessary that the sensing network attenuates the low-frequency components of the measured voltage. A value of approximately -40-dB attenuation for the 50-Hz component would imply that, for a 300-V peak in the line-to-ground (PE) voltage, a peak voltage of 3 V appears in the output of the power amplifier. In this case, a minimum attenuation of -50 dB at 50 Hz was chosen as a starting point.

Another specification is that the high-frequency gain should be practical with a low-cost HF power amplifier. This specification also matches the gain limitation imposed by the plant's characteristics. The actuator for the proposed system is a linear HF power amplifier with a transfer function G_{amp} presenting enough bandwidth in order to allow a good performance. A good model for such amplifier is a first-order low-pass filter with a limited output swing due to the available supply voltage.

The most simple and desirable way to sense the voltage u_F is to use a high-pass filter. In the case at hand, it is composed of two zeros, one at the origin and the other above 10 kHz. This results in a high attenuation of the 50/60-Hz component.

Poles are placed at high frequency in order to limit the high-frequency gain. The final bandwidth of the feedback loop must be limited due to the power-amplifier characteristics. This is achieved by placing a dominant pole at a frequency where the high-frequency gain is rolled-off correctly, thus guaranteeing that the design is carried out with the assumption that the amplifier behaves like an ideal operational amplifier.

$$\frac{I_f(s)}{U_o(s)} = \frac{s^3 L_g C_f C_o (s^2 C_s L_s + 1)}{s^4 L_g L_s C_s (C_f + C_o) + s^2 \left[L_g (C_f + C_o - C_s) + L_s C_s\right] + 1} \tag{2}$$

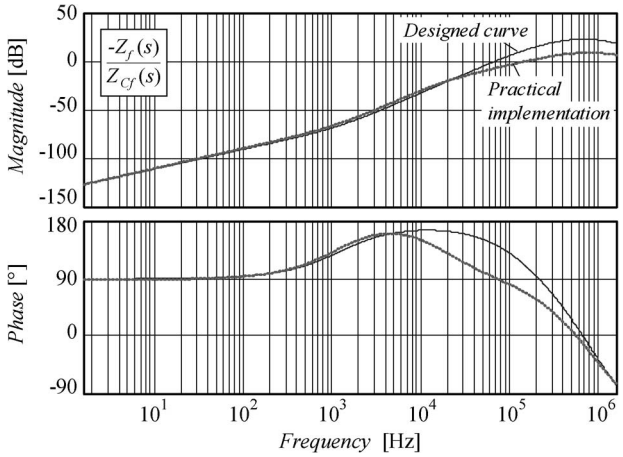

Fig. 8. Bode diagrams for the designed feedback loop (cf. Fig. 9). The high-frequency gain for the practical implementation was lowered due a nonideal characteristic of the HF power amplifier not accounted for in the model.

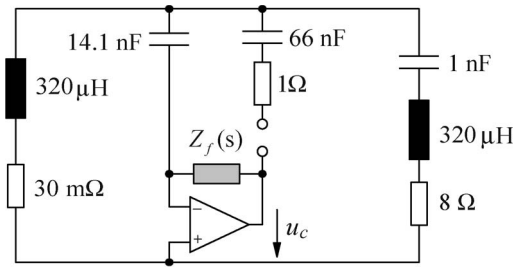

Fig. 9. Circuit used for the transmission-loop calculations and the employed transfer function $Z_f(s)$. Parasitic resistances from inductors and load have been estimated through impedance measurements, and the output resistance of the amplifier is estimated through circuit simulation of the designed amplifier shown in Section IV.

Defining the sensing capacitor impedance as

$$Z_{Cf}(s) = \frac{1}{s\,C_f} \tag{3}$$

the designed feedback loop, $-Z_f(s)/Z_{Cf}(s) = U_c(s)/U_f(s)$, for an ideal operational amplifier can be observed in Fig. 8. A curve for the designed loop and another curve for the actual performance of the finally implemented system are shown. The maximum slew rate of the implemented power amplifier prevented higher gains to be applied in practice because it distorts the output signal in a way that the high-frequency components are attenuated and phase shifted nonlinearly. This reduction in the HF gain limits the final achievable attenuation increase.

Considering the amplifier nonidealities as a transfer function $G_{\rm amp}(s)$, the transfer function $U_c(s)/I_f(s)$ is given by

$$\frac{U_c(s)}{I_f(s)} = -Z_f \frac{G_{\rm amp}(s)}{1 + G_{\rm amp}(s)} \tag{4}$$

from where it is seen that it impacts the HF behavior of the designed active filter.

The final control-oriented block diagram for the circuit of Fig. 9 of the designed system is shown in Fig. 10, where the influence of the amplifier transfer function is simplified just for the sake of clarity (respective bode plots are presented in

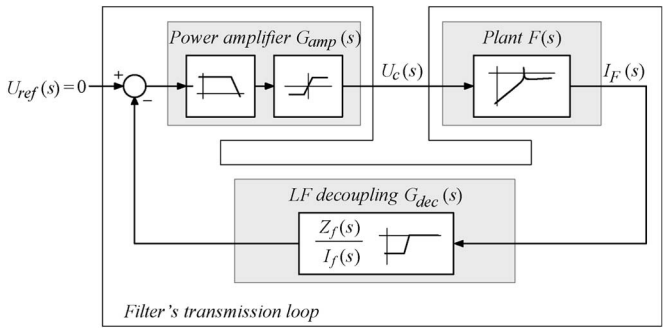

Fig. 10. Filter's transmission-loop block diagram.

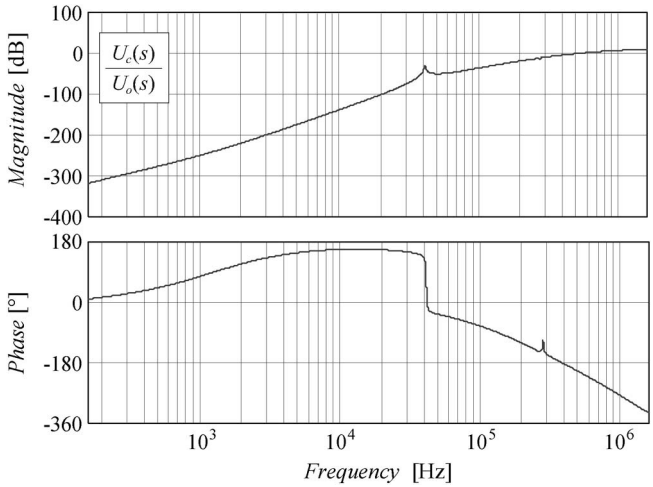

Fig. 11. Bode plots for the modeled transmission loop including resistive elements estimated from impedance measurements and the high-frequency pole modeling the power amplifier $G_{\rm amp}$.

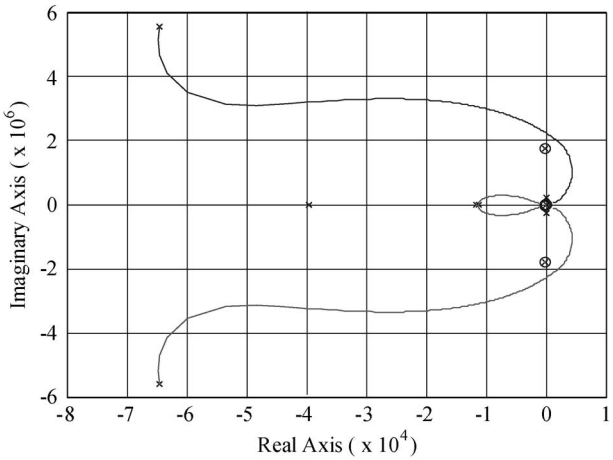

Fig. 12. Root-locus diagram for the designed system, which is shown in Fig. 9.

Fig. 11). This is used to obtain the final root-locus diagram of the transmission loop which is shown in Fig. 12. The inductors are modeled here as a constant inductor in series with a resistance, allowing the system stability to be analyzed with mathematical tools for linear systems. With the previously shown feedback structure, the determining part of the root locus is the region close to the origin, which includes the low-frequency zeros and the dominant complex poles. The design

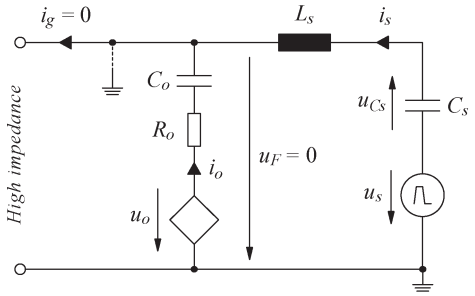

Fig. 13. Simplified circuit for studying the requirements for an HF power amplifier to be used in active mains filtering. Noise source: u_s in series with C_s; amplifier output: u_o, and output resistance R_o.

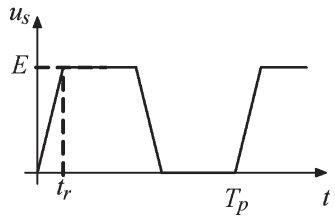

Fig. 14. Considered waveform at the noise source.

ensures that large values of mains and noise-source impedances can be employed. The final system has been successfully tested with noise-source capacitances ranging from 10 pF up to 10 μF and mains-sided impedances from around 100 nH up to 12 mH measured at 1 kHz. Furthermore, the design ensures that if minimum values for the inductors $L_{CM,1}$ and $L_{CM,2}$ are employed, system stability is given for widely varying external impedances.

IV. Amplifier Design

The main points in specifying the amplifier are the following: 1) dc supply voltage; 2) power bandwidth; and 3) power supply rejection ratio. Since costs are typically important, a tradeoff between costs and performance is usually required as well.

To start with, the circuit of Fig. 13 is considered, where u_s in series with C_s represents a noise source, inductance L_s is the first filter inductor, and the branch formed by C_o is the filter capacitance; u_c is the output voltage of the power amplifier with an output impedance R_o limited by the resistors connected at the amplifier output. The remainder of the circuit is neglected. The aim is to generate a voltage waveform at u_c capable of injecting a compensating current, which should keep the voltage at the node between L_s and C_o as close as possible to the ground potential 0 V, thus current i_g should equal zero.

Two simplifying assumptions are made: 1) the noise voltage source u_s is a trapezoidal shape with an amplitude E and a finite rise time t_r as shown in Fig. 14, and 2) u_f equals zero. From circuit inspection, the following ordinary differential equations are derived:

$$L_s \frac{di_s}{dt} = u_s - u_{Cs} \tag{5}$$

$$C_s \frac{du_{Cs}}{dt} = i_s \tag{6}$$

$$C_o \frac{du_c}{dt} = i_o + C_o R_o \frac{di_o}{dt}. \tag{7}$$

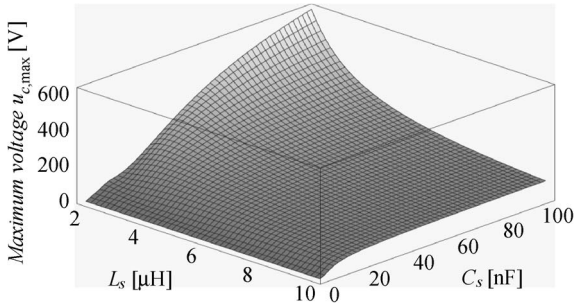

Fig. 15. HF power amplifier requirement translated into dc supply voltage $V_{cc} = u_{c,\max}$, for $C_o = 66$ nF, $R_o = 1\ \Omega$, and $E = 400$ V, where $u_{c,\max}$ is shown as a function of noise-source capacitance C_s and inductance L_s for ideal compensation and $t_r = 1\ \mu$s.

Equations (5) and (6) represent the circuit branch in which the noise current i_s is generated. Assuming the initial conditions

$$i_s(0) = 0 \tag{8}$$

$$u_{Cs}(0) = 0 \tag{9}$$

the solution for i_s for the ordinary differential equations system formed by (5) and (6) is given by

$$i_s(t) = C_s \frac{E}{t_r}\left[\cos\left(\frac{t}{\sqrt{L_s C_s}}\right) - 1\right]. \tag{10}$$

Considering the other branch of the circuit, the circuit is characterized by (7). The initial condition for this circuit is assumed as

$$i_o(0) = 0. \tag{11}$$

Solving (7) for (11) leads to

$$\frac{du_c}{dt} = \frac{i_o(t)}{C_o\left(e^{\frac{-t}{\sqrt{C_o R_o}}} - 1\right)}. \tag{12}$$

The condition which should be fulfilled is

$$i_o(t) = -i_s(t). \tag{13}$$

Assuming $R_o = 0\ \Omega$, inserting (13) into (12) and solving the equation for du_c/dt, the output voltage of the amplifier u_o must be able to achieve the following parameters:

$$\frac{du_{c,\max}}{dt} = \frac{C_s}{C_o}\frac{E}{t_r}\frac{\cos\left(\frac{t}{\sqrt{L_s C_s}}\right)}{\left(e^{\frac{-t}{\sqrt{C_o R_o}}} - 1\right)} \tag{14}$$

$$u_{c,\max} = \int_0^{t_r} \frac{C_s}{C_o}\frac{E}{t_r}\frac{\cos\left(\frac{t}{\sqrt{L_s C_s}}\right)}{\left(e^{\frac{-t}{\sqrt{C_o R_o}}} - 1\right)} dt. \tag{15}$$

Equations (14) and (15) define the requirements for ideal cancellation, based on the given simplifications, and, with this, it is possible to evaluate the requirements for an amplifier given specific circuit parameters as shown graphically in Figs. 15 and 16, where the surfaces for the required dc supply voltage

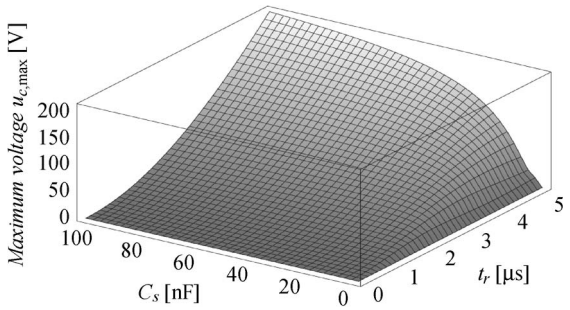

Fig. 16. HF power amplifier requirements translated into dc supply voltage $V_{cc} = u_{c,\max}$, for $C_o = 66$ nF, $R_o = 1\ \Omega$, and $E = 400$ V, where $u_{c,\max}$ is a function of noise-source capacitance C_s and rise time t_r for ideal compensation and $L_s = 100\ \mu$H.

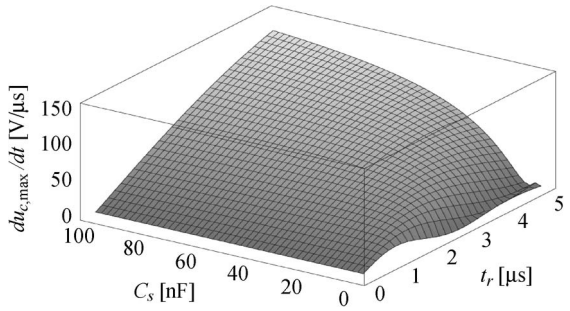

Fig. 17. HF power amplifier requirements translated into maximum voltage-change ratio $d_{uc,\max}/dt$, for $C_o = 66$ nF, $R_o = 1\ \Omega$, and $E = 400$ V, where $d_{uc,\max}/dt$ is a function of noise-source capacitance C_s and rise time t_r for ideal compensation and $L_s = 100\ \mu$H.

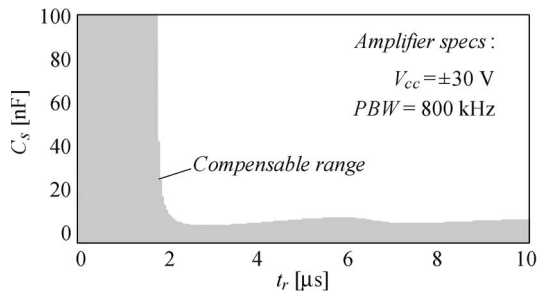

Fig. 18. (Shaded region) Compensable range valid for $L_s = 100\ \mu$H for an amplifier with $V_{cc} = \pm 30$ V and $PBW = 800$ kHz.

$V_{cc} = u_{c,max}$ are displayed for a perfect compensation of the noise-source voltage. An example for maximum voltage ratio $du_{c,max}/dt$ surface is shown in Fig. 17, translating in the requirement for the amplifier power bandwidth PBW. In Fig. 18, the range where an ideal noise compensation can be achieved is shown, given the specified amplifier and circuit parameters.

Based on the given requirements and aiming for a prototype to be used with a "state-of-the-art" three-phase ASD based on a 6.8-kVA SMC, where the switching times are usually under 500 ns and the switching frequency $f_P = 10/20$ kHz, it seems to be adequate that an amplifier with a dc supply of $V_{cc} = \pm 30$ V and a power bandwidth of $PBW = 800$ kHz is employed. A discrete HF power amplifier as shown in Fig. 19 was designed and built for a system being fed with a ±30-V external power supply. The amplifier is built with conventional surface-mount-device (SMD)-type components (cf. Table I) and exhibits a closed-loop −3-dB bandwidth of approximately 1 MHz and a power bandwidth of approximately 800 kHz.

V. Practical Implementation of the Active Filter

A three-phase filter employing the presented feedback structure was built in order to test the presented mathematical models. The filter schematics are shown in Fig. 20 and the main components are specified in Table I. The filter employs inductors built with nanocrystalline cores (VAC VITROPERM 500F), which have a highly resistive behavior at high frequencies, helping to ensure high impedances at high frequencies, a well-damped self-resonance, and a good thermal stability. The inductor models account for the complex permeability curves from the manufacturer and the parallel parasitic capacitances. The capacitor models include capacitance, equivalent series resistance, and inductance as given in the datasheet [27].

In hand of this modeling, the filter-insertion-loss (50-Ω input/50-Ω output measurement) curves for the designed filter were calculated as shown in Fig. 21, where the curve for the filter without feedback can be compared with real measurement data (indicated by crosses) and a good agreement is observed, except for a structural resonance[1] at approximately 20 MHz. Based on the modeled components, two simulations were performed, and their results are also shown in Fig. 21. The first simulation, shown in the middle trace of Fig. 21, gives the filter-insertion loss in the case where a band-limited amplifier is used, showing that an increase in the attenuation is observed up to the amplifier's frequency limitation. The last simulation, bottom trace, is valid for an infinite-bandwidth amplifier. The potential for such systems is clear, and with larger amplifier bandwidth, better performance is observed. Based on the successful simulation results, a prototype based on the structure shown in Fig. 20 was built. The prototype is rated for 10 A/400 V/50 Hz, and a photograph is shown in Fig. 22.

The first step in the prototype testing was to analyze the system stability under different source and load impedances. Inductors with ferrite cores of 1 and 6 mH and inductors with nanocrystalline cores of 4.2 and 12 mH, measured at 1 kHz, were used as artificial mains and/or source impedances. On the noise-source side, capacitors in the range of 10 pF up to 10 μF were employed. Short-circuiting of the filter inputs to PE was also tested. Over this impedance range, the filter operated in a stable manner. Attenuation measurements were also performed employing different source and load impedances. Fig. 23 shows the measurement for an 8-Ω input impedance and a 50-Ω output for the filter structure with and without (C_f and $C_{o,i}$ shorted to PE) active feedback. The same measurements were repeated for a 4.2-mH source impedance, and the results are shown in Fig. 24, showing the increase in the filter attenuation in the range of 100 kHz to 1 MHz, where the amplifier bandwidth ends.

Another performed test made use of a square-wave generator as noise source in series with a 400-pF SMD capacitor mounted on a printed circuit board (PCB) with a very small space

[1]This resonance has not been clarified in practice because of its minor effects observed in the transfer functions.

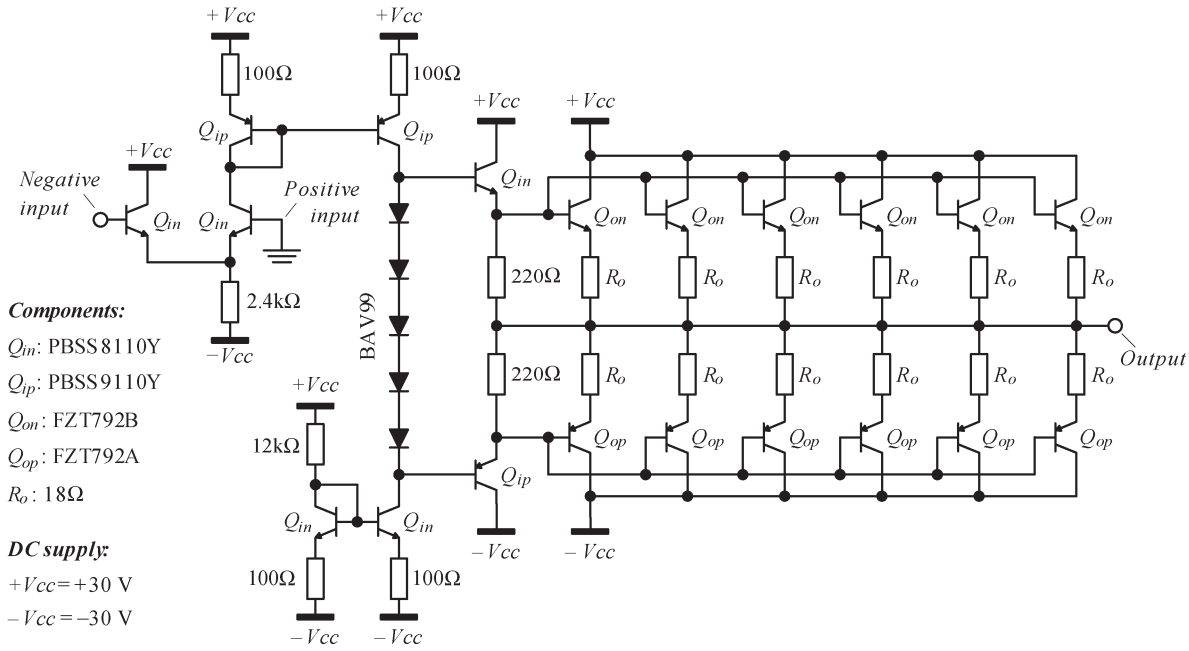

Fig. 19. Schematic of employed linear HF power amplifier. The topology is selected aiming for low implementation costs.

TABLE I
SELECTED COMPONENTS FOR THE ACTIVE FILTER PROTOTYPE

Component	*Specification*
$C_{f,i}$	Y2 SMD Capacitor, Murata X7R Series GC 4.7 nF – 250 Vac
$C_{o,i}$	Y2 Capacitor, Epcos MKP B81122 22 nF – 250 Vac
$C_{CM,i}$	Y2 SMD Capacitor, Murata X7R Series GC 1 nF – 250 Vac
$L_{CM,1}$	Vaccuumschmelze VAC VITROPERM 500F T6000-6-L2012-W498 – OD(12.5) ID(10) H(5) mm N = 3 × 3 turns, ϕ 1 mm
$L_{CM,2}$	Vaccuumschmelze VAC VITROPERM 500F T6000-6-L2012-W498 – OD(12.5) ID(10) H(5) mm N = 3 × 4 turns, ϕ 1 mm

between the capacitor and the ground plane in the backside of the PCB. As load, a four-line 50 Ω/50 μH V-network LISN was used and its output was connected to an EMC test receiver. Measurements with and without filter are shown in Fig. 25. For the measurement with the active feedback, it is demonstrated that higher attenuation is achieved up to 1 MHz. At 2 MHz, a resonance in the amplifier circuit due to the distortion caused by its slew-rate limitation is seen, causing higher emission levels than those of the filter without feedback. In the higher frequency range, the same conducted emission levels are seen.

The last presented test is performed with the active-filter board connected at the input of an ASD built on a 6.8-kVA SMC. The SMC board has three SMD Y-capacitors of 4.7 nF connecting each phase terminal to the PE. The load of the SMC is an RL load that is not connected to PE. A four-line 50 Ω/50 μH V-network LISN was used with its outputs connected to a three-phase noise separator and then to an EMC test receiver. Measurements performed with the noise separator CM output, with and without filter, are shown in Fig. 26. For the measurement with the active feedback, it is clear that higher attenuation is achieved up to 500 kHz. In the higher frequency range, the same conducted emission levels are seen; therefore, the active filter does not influence this range. As a larger CM inductor is present at the input of the SMC, due to high CM voltages and for this reason, lower gain in attenuation is achieved, but this proves that the active filter can be used interfacing the grid and an ASD.

Given the achieved results and considering a normative measurement frequency range from 150 kHz to 30 MHz, it is clear that the performance improvements to frequencies higher than 2 MHz are to be cogitated. Thus, further investigations on higher bandwidth amplifiers, components with reduced parasitics, and improved packaging/layout are to be considered. However, the tradeoffs between the costs of more elaborate solutions and their benefits must be analyzed.

VI. LOW-FREQUENCY REJECTION POSING LIMITATIONS IN ACTIVE-FILTER PERFORMANCE

From the results presented in the previous sections, it can be seen that the attenuation improvement with the designed active filter was not 40 dB, as typically desired and sometimes demonstrated in some experimental applications [11], [20]. It is found that when a high-pass filter is applied at the feedback loop, the HF feedback gain shall be limited in order to guarantee stability for a wide and practical range of mains impedance. To acquire an insight into the limitations to the gain in attenuation some theoretical studies are carried out in the following for different active-filter structures, represented through simplified models. The mains impedance is here modeled as an inductor with a value of $L_g = 50$ μH for all cases.

1) Voltage Sensing/Current Actuation (VSCA) Filter With Passive Damping: The circuit of Fig. 27 is used, where the network composed of L_d and R_d provide passive damping to the circuit, thus possibly allowing for higher feedback gains. This is, of course, not practical since access to the mains impedance would be required. On the other hand, it is useful

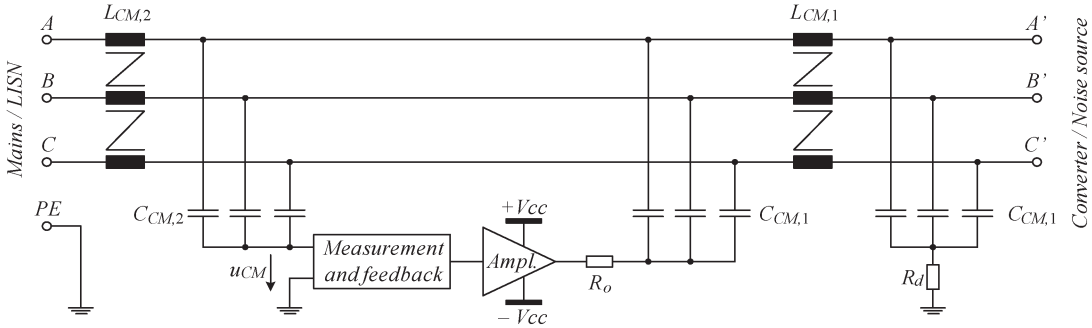

Fig. 20. Circuit schematic for the designed filtering system. Components are specified in Table I.

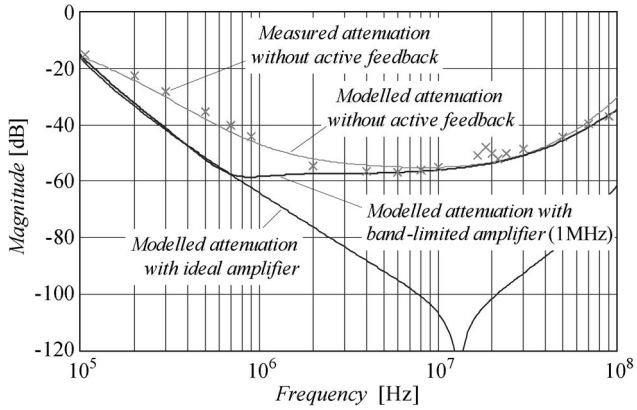

Fig. 21. Insertion-loss curves (50-Ω input/50-Ω output measurement) for different feedback structures. The crosses represent real measurements on the built filter board with no active feedback, while the top trace shows the insertion loss for the mathematically modeled filter. The middle curve shows the expected behavior when utilizing an active feedback, which makes use of a band-limited power amplifier, while the lower curve shows the performance with the circuit employing an infinite-bandwidth amplifier.

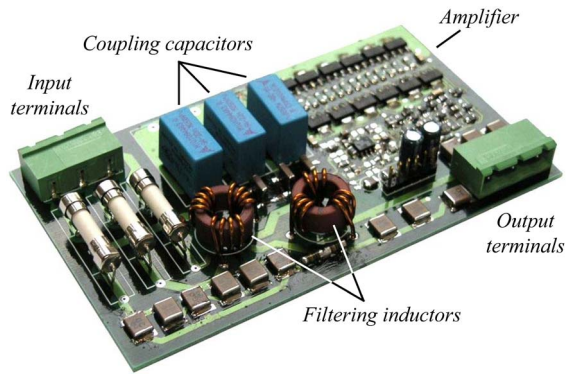

Fig. 22. Three-phase filter prototype photograph ($120 \times 70 \times 17$ mm^3).

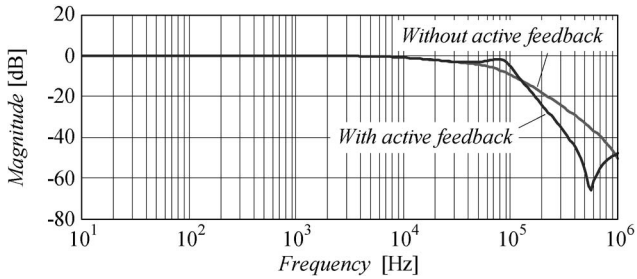

Fig. 23. Performance for the designed filter with a source impedance of approximately 8 Ω. Measured attenuation curves for a load impedance of 50 Ω.

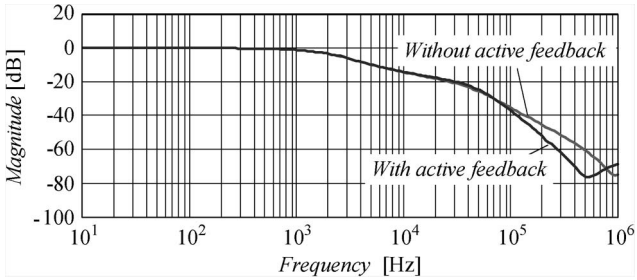

Fig. 24. Performance of the designed filter with a source impedance of approximately 4.1 mH (measured at 1 kHz). Measured attenuation curves for a load impedance of 50 Ω.

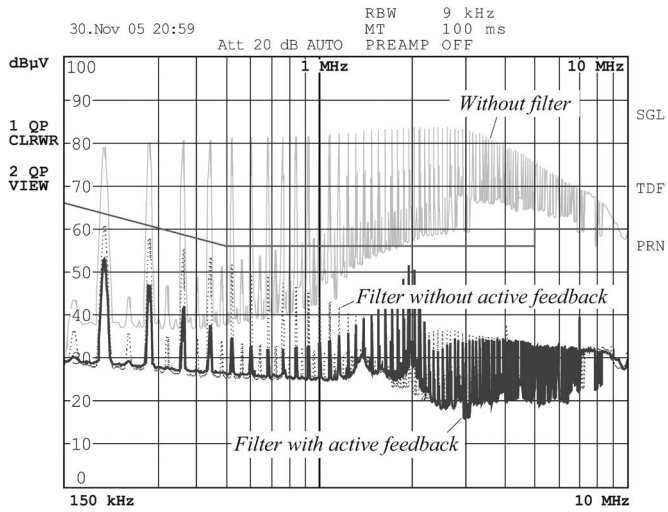

Fig. 25. Conducted emission measurements performed employing a square-wave generator switching at 40 kHz with a rise/fall time of around 30 ns in series with a capacitance of approximately 400 pF. Upper trace shows the emission levels without a filter. Dashed trace shows the measurement result with no active feedback. Third trace presents the results when the proposed electronic feedback is active.

in order to gain insight about the stringent requirements for the feedback design.

As a starting point, some assumptions are made.

1) The noise source is modeled as a current source i_s.
2) The sensing network $G_{\text{sens}}(s)$ shall provide more than a 40-dB attenuation at 50 Hz. This is achieved with a second-order high-pass filter defined as

$$G_{\text{sens}}(s) = \frac{100s^2}{s^2 + 53855.9s + 1.4212 \cdot 10^9}. \qquad (16)$$

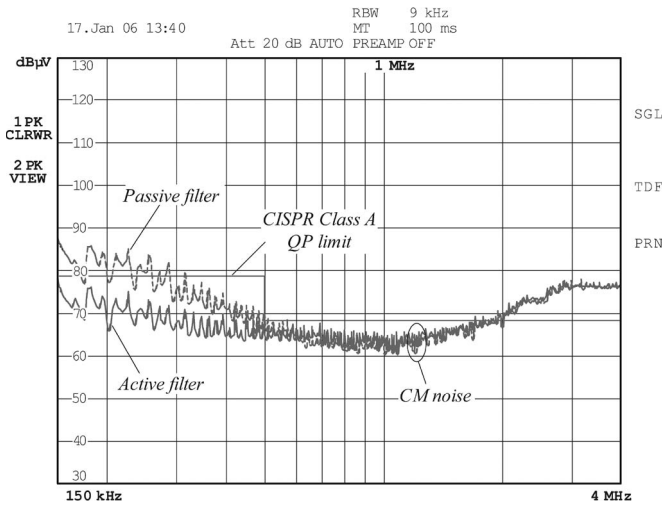

Fig. 26. CM conducted emission measurements (acquired with the help of a three-phase CM/differential mode noise separator as in [28]) performed on a three-phase ASD based on a 6.8-kVA SMC, switching frequency $f_P = 10/20$ kHz. Dashed upper trace shows the emission levels without the active feedback. Full trace shows the measurement result with the electronic feedback active.

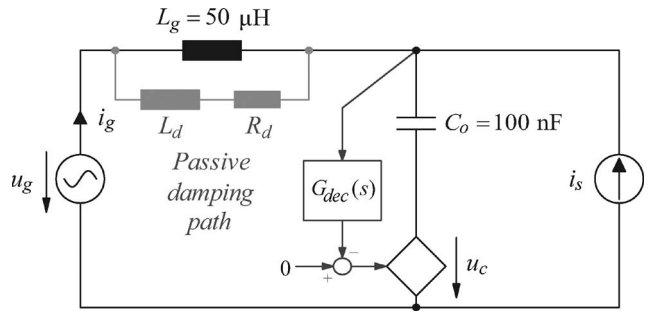

Fig. 27. Analyzed circuit for a VSCA active filter with passive damping.

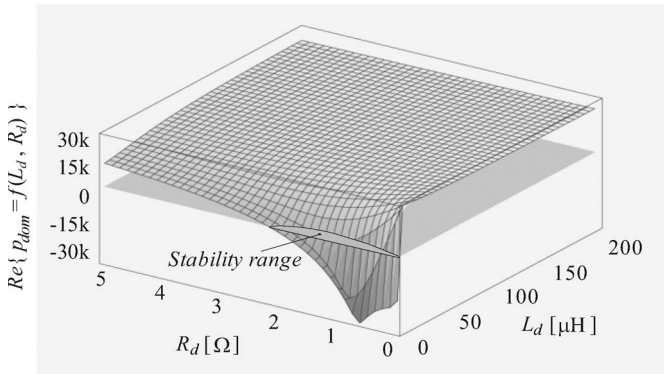

Fig. 28. Real part of the dominant complex-conjugated poles as a function of the passive damping network impedances L_d and R_d for a VSCA active filter with passive damping.

3) The HF gain in attenuation for the active filter shall be around 40 dB, when compared with a passive filter with the same components.
4) The circuit should be stable.

Based on the listed requirements and on the circuit of Fig. 27, the real part of the complex-conjugated dominant poles of the open-loop transfer function are plotted in Fig. 28, where it is seen that only a very limited range of impedances L_d and R_d drive the real part of the dominant poles to the negative region, leading to stable operation modes. This can be interpreted as a maximum equivalent mains impedance in order to achieve a gain of 40 dB in attenuation with active feedback. Values for L_d and R_d inside the stable range are taken in order to plot the attenuation $I_g(s)/I_s(s)$ curves (cf. Fig. 29), from which it is seen that the active filter achieves an attenuation around 40 dB higher than the passive one for HF.

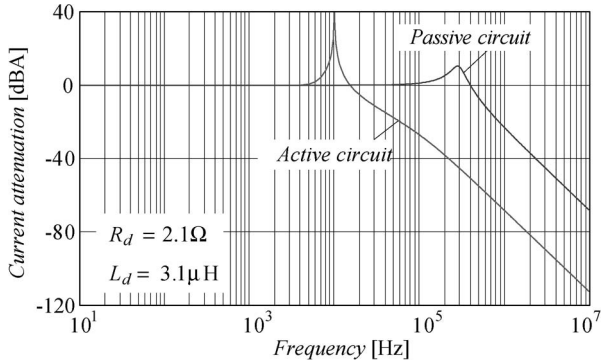

Fig. 29. Current attenuation curves for $L_d = 3.1$ μH and $R_d = 2.1$ Ω showing a gain of 40 dB for HF from the active to the passive filter for a VSCA active filter with passive damping.

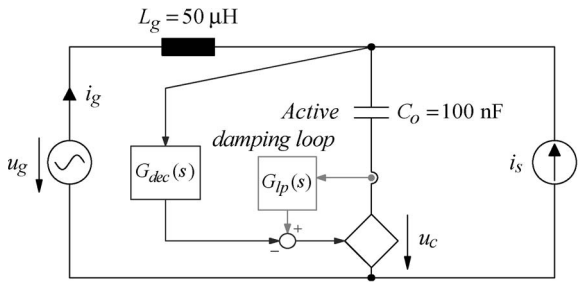

Fig. 30. Analyzed circuit for a VSCA active filter including an active damping loop.

2) Voltage Sensing/Current Actuation (VSCA) Filter With Active Damping: As the concept of passively damping the network impedance is impractical, the theoretical use of active damping is analyzed. An active-damping loop is added to the circuit by sensing the current through capacitor C_o and feeding it back positively to the amplifier. As a drawback, HF current sensing has to be implemented. The circuit of Fig. 30 shows the basic implementation. With this scheme, however, it is not possible to guarantee the increase of attenuation by 40 dB using the active circuit instead of the passive network as there might be a limit as a consequence of the stability analysis. The following assumptions are made.

1) The noise source is modeled as a current source i_s.
2) The feedback $G_{\rm sens}(s)$ shall provide more than 40 dB attenuation at 50 Hz. This is achieved with a second-order high-pass filter.
3) The HF gain in attenuation for the active filter must be as large as possible.
4) The circuit must be stable.

Since a closed-form solution cannot be derived due to the large number of variables and the nontrivial form of the involved equations, numerical optimization is utilized. The objective function is the HF gain of the feedback loop and the

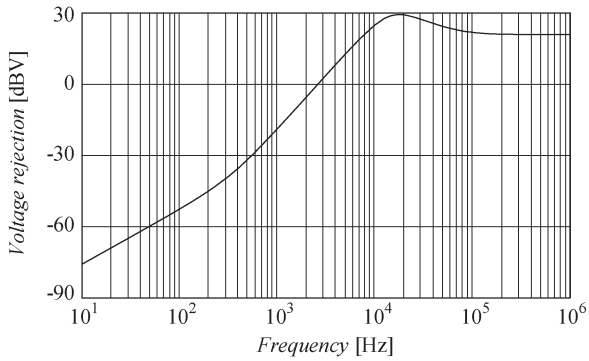

Fig. 31. Voltage rejection/gain for the amplifier of a VSCA active filter including an active damping loop.

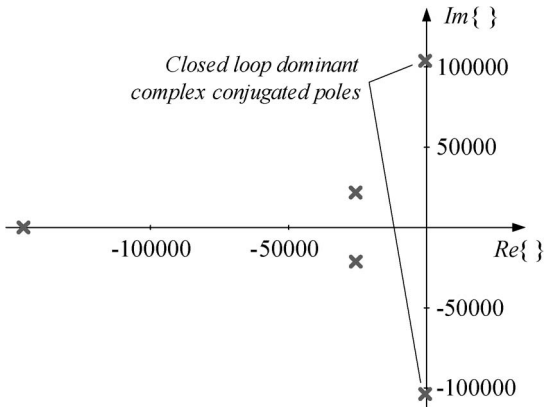

Fig. 32. Root locus showing the position of the closed-loop system poles of a VSCA active filter including an active damping loop.

constraints are the 50-Hz voltage rejection and the stability. This transforms the problem into a nonconvex one. To solve the problem, the "Global Optimization Toolbox" of the software "Maple 10" has been used. The four optimized variables were the corner frequencies and the gains of the feedback transfer functions $G_{\rm dec}$ and G_{lp}, given by

$$G_{\rm dec}(s) = \frac{57.38s^2}{s^2 + 54143.1s + 1.4364 \cdot 10^9} \tag{17}$$

$$G_{lp}(s) = \frac{176}{5.0686 \cdot 10^9 s + 1}. \tag{18}$$

The optimization results have led to the following results. Fig. 31 shows that the 50-Hz rejection is above the required 40 dB. The position of the closed-loop poles in the complex plane (cf. Fig. 32) demonstrates that the system is stable. Thus, both constraints are fulfilled. Through the attenuation curves (cf. Fig. 33), it is clear that a gain in attenuation of 40 dB is not achieved. Although there is not a 100% certainty that the global optimum was achieved, it is very difficult that a substantially improved solution is possible for these type of structures. Thus, for the specified problem, a maximum gain of around 20 dB is to be expected. Another interesting result is the action of the active-damping loop, which can be observed in the effect of the feedback loops in the impedance of the parallel circuit branch formed by u_c and C_o (cf. Fig. 34). The impedance curve shows that a resistive section around 10 kHz is observed, which damps the final closed-loop system.

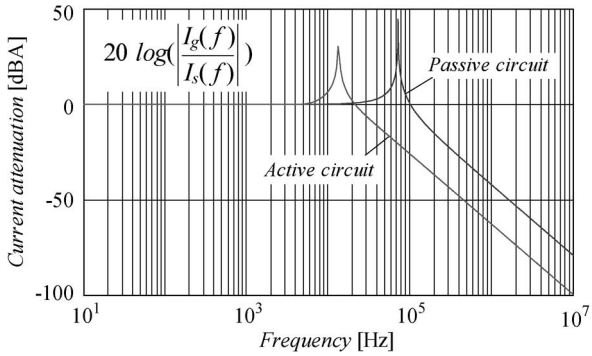

Fig. 33. Active- and passive-filter current-attenuation curves showing around 20 dB gain in attenuation for HF for a VSCA active filter including an active damping loop.

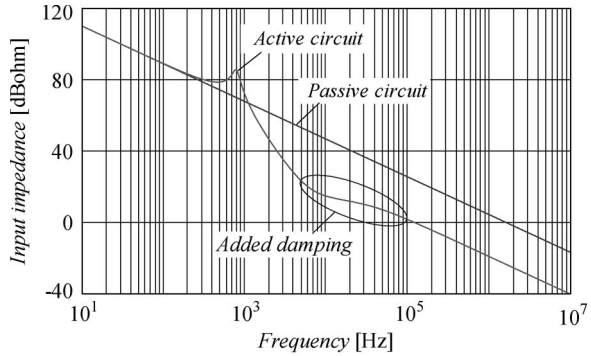

Fig. 34. Parallel branch (u_c and C_o) impedance magnitude curves for the active and passive circuits for a VSCA active filter including an active damping loop.

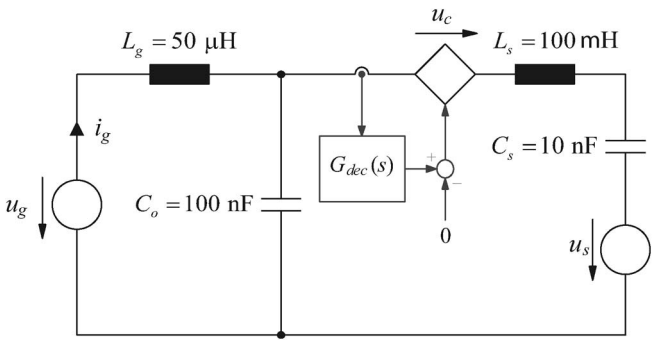

Fig. 35. CSVA.

3) Other Active-Filter Structures: Based on the procedure and requirements presented in Section VI-A-2, similar studies have been performed for the other active-filter structures.

The structure of a "Current Sensing/Voltage Actuation"—CSVA—topology is shown in Fig. 35. The attenuation-curve results for this structure, achieved with numerical optimization are displayed in Fig. 36.

The structure of a "Voltage Sensing/Voltage Actuation"—VSVA—topology is shown in Fig. 37. The attenuation-curve results for this structure, achieved with numerical optimization are displayed in Fig. 38.

The structure of a "Current Sensing/Current Actuation"—CSCA—topology is shown in Fig. 39. The attenuation curve

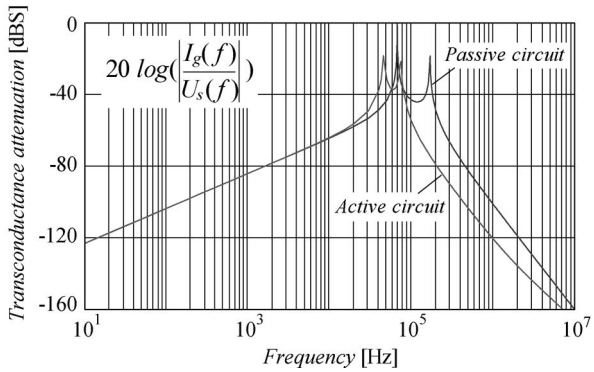

Fig. 36. Attenuation curves for the filter structures of Fig. 35 (CSVA) achieved with numerical optimization.

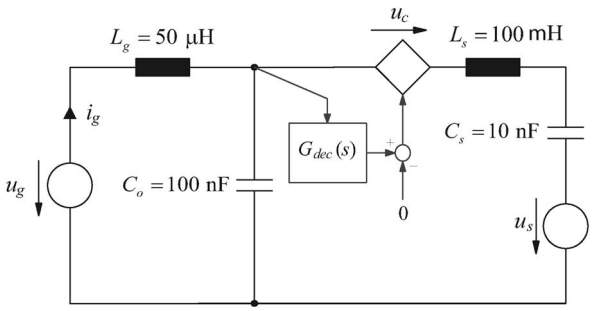

Fig. 37. VSVA.

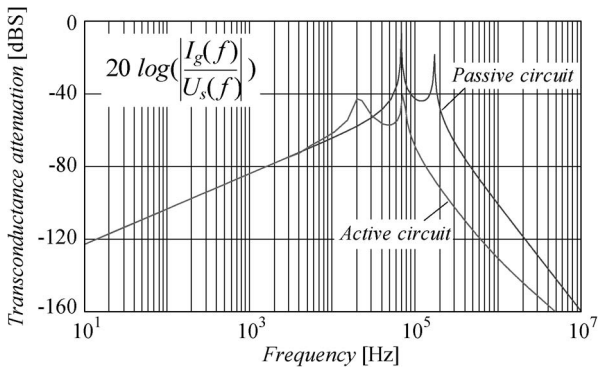

Fig. 38. Attenuation curves for the filter structures of Fig. 37 (VSVA) achieved with numerical optimization.

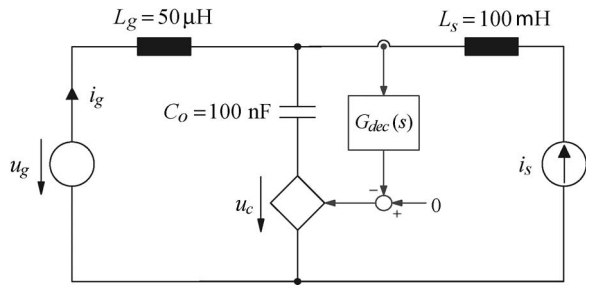

Fig. 39. CSCA.

results for this structure, achieved with numerical optimization are displayed in Fig. 40.

From the presented attenuation-curve results, the gains in attenuation, with the application of feedback, range from 20 to

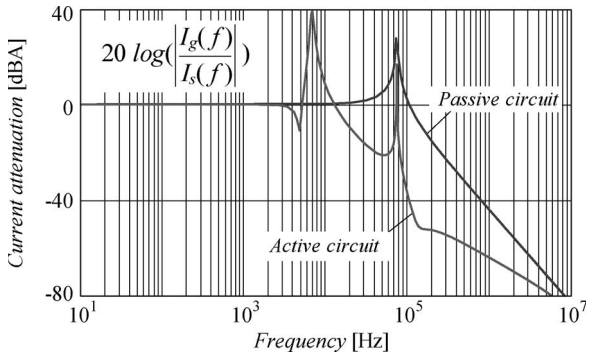

Fig. 40. Attenuation curves for the filter structures of Fig. 39 (CSCA) achieved with numerical optimization.

30 dB. These results show that high-attenuation enhancements are very difficult to achieve with the application of second-order high-pass filters in the feedback paths. This type of structure, therefore, imposes limitations for the application of active filters connected directly to the mains. On the other hand, applications where the source and load impedances are well defined and/or where such a high attenuation of low-frequency components is not required, such as dc supplied converters, do not suffer from the same stability restrictions and can, therefore, present more sensible performance improvements.

VII. Conclusion

An implementation strategy for an HF-amplifier-based CM active filter for offline converter systems has been proposed. For such a system, the low-frequency (50/60 Hz) attenuation in the feedback loop is of high importance in order to prevent amplifier saturation. However, this limits the filter's operating-frequency range.

A literature survey has indicated the possible filter structures, by identifying the critical issues and main advantages for the selected approach. The designed filter is based on capacitive coupling for both sensing and actuation, eliminating the need for HF transformers. General requirements for an HF power amplifier to be used in active filtering have been derived.

The active-filter function has been explained in detail and a stability-analysis procedure has been presented which is carried out with reference to root-locus diagrams and simplified circuit models. A feedback design for the selected filter topology, which fulfills the stability requirements for the system and is characterized by a higher filter attenuation and/or smaller passive filter components, has been proposed.

The presented simulation and practical results demonstrate that this system has potential for practical use, although limitations in increasing attenuation are shown. Large attenuation for high frequencies is limited due to the highly reactive nature of the filter structure, but the use of a higher bandwidth amplifier would lead to better results. Based on the potential of this technique, other types of feedback structure have been studied in their principles. Due to stability reasons, the analyzed structures are characterized by limitations in the gain of attenuation which can be achieved with an active filter having a high-pass filter in its feedback loop.

REFERENCES

[1] H. Hsieh, J.-S. Li, and D. Chen, "Effects of X capacitors on EMI filter effectiveness," *IEEE Trans. Ind. Electron.*, vol. 55, no. 2, pp. 949–955, Feb. 2008.

[2] J. Walker, "Designing practical and effective active EMI filters," in *Proc. Powercon 11*, 1984, vol. I-3, pp. 1–8.

[3] L. LaWhite and M. F. Schlecht, "Active filters for 1-MHz power circuits with strict input/output ripple requirements," *IEEE Trans. Power Electron.*, vol. PE-2, no. 4, pp. 282–290, Oct. 1987.

[4] L. LaWhite and M. F. Schlecht, "Design of active ripple filters for power circuits operating in the 1–10 MHz range," *IEEE Trans. Power Electron.*, vol. 3, no. 3, pp. 310–317, Jul. 1988.

[5] T. Farkas and M. F. Schlecht, "Viability of active EMI filters for utility applications," *IEEE Trans. Power Electron.*, vol. 9, no. 3, pp. 328–337, May 1994.

[6] W. Chen, X. Yang, and Z. Wang, "Analysis of insertion loss and impedance compatibility of hybrid EMI filter based on equivalent circuit model," *IEEE Trans. Ind. Electron.*, vol. 54, no. 4, pp. 2057–2064, Aug. 2007.

[7] K. Hironobu and F. Katsumi, "Active filter," Japan Patent 087 973, 2003.

[8] Y. C. Son and S. Seung-Ki, "A new active common-mode EMI filter for PWM inverter," *IEEE Trans. Power Electron.*, vol. 18, no. 6, pp. 1309–1314, Nov. 2003.

[9] E. V. Larsen and R. Delmerico, "Hybrid active power filter with programmed impedance characteristics," U.S. Patent 5 737 198, Apr. 7, 1998.

[10] B. Pelly, "Active common mode filter connected in A-C line," U.S. Patent 6 690 230, Feb. 10, 2004.

[11] S. Ogasawara, H. Ayano, and H. Akagi, "An active circuit for cancellation of common-mode voltage generated by a PWM inverter," *IEEE Trans. Power Electron.*, vol. 13, no. 5, pp. 835–841, Sep. 1998.

[12] S. Ogasawara and H. Akagi, "Circuit configurations and performance of the active common-noise canceller for reduction of common-mode voltage generated by voltage-source PWM inverters," in *Conf. Rec. IEEE IAS Annu. Meeting*, 2000, vol. 3, pp. 1482–1488.

[13] M. C. Di Piazza, G. Tine, and G. Vitale, "An improved active common-mode voltage compensation device for induction motor drives," *IEEE Trans. Ind. Electron.*, vol. 55, no. 4, pp. 1823–1834, Apr. 2008.

[14] A. C. Chow and D. J. Perreault, "Active EMI filters for automotive motor drives," in *Proc. Power Electron. Trans.*, 2002, pp. 127–134.

[15] Y. Kanehara, "Noise filter," Japan Patent 244 770, 2001.

[16] J. Honda, "Active EMI filter having no inductive current sensing device," International Patent 109 896, 2004.

[17] J. Honda, "Active EMI filter," International Patent 001 927, 2004.

[18] D. Y. Lee and B. H. Cho, "Design of an input filter for power factor correction (PFC) AC to DC converters employing an active ripple cancellation," in *Proc. Intersociety Energy Conversion Eng. Conf.*, 1996, vol. 1, pp. 582–586.

[19] M. Zhu, D. Perreault, V. Caliskan, T. Neugebauer, S. Guttowski, and J. Kassal, "Design and evaluation if an active ripple filter with Rogowski-coil current sensing," in *Proc. IEEE Power Electron. Spec. Conf.*, 1999, vol. 2, pp. 874–880.

[20] J. Dumas, B. Lanoue, and B. Tahhan, "Active analog power filters provide solutions for EMC and EMI," in *Proc. IEEE Appl. Power Electron. Conf. Expo.*, 2004, vol. 2, pp. 675–680.

[21] B. Pelly, "Active filter for reduction of common mode current," U.S. Patent 6 636 107, Oct. 21, 2003.

[22] J. R. Nicholson and J. A. Malack, "RF impedance of power lines and line impedance stabilization networks in conducted interferences measurement," *IEEE Trans. Electromagn. Compat.*, vol. EMC-15, no. 2, pp. 84–86, May 1973.

[23] J. P. Rhode, A. W. Kelley, and M. E. Baran, "Line impedance measurement: A nondisruptive wideband technique," in *Conf. Rec. IEEE IAS Annu. Meeting*, 1995, vol. 3, pp. 2233–2240.

[24] S. Wang, J. D. van Wyk, and F. C. Lee, "Effects of interactions between filter parasitics and power interconnects on EMI filter performance," *IEEE Trans. Ind. Electron.*, vol. 54, no. 6, pp. 3344–3352, Dec. 2007.

[25] CISPR, C.I.S.P.R. Specification for Radio Interference Measuring Apparatus and Measurement Methods—Publication 16, Geneva, Switzerland: IEC Int. Spec. Committee Radio Interference—C.I.S.P.R., 1977.

[26] G. F. Franklin, J. D. Powell, and A. Emani-Naemi, *Feedback Control of Dynamic Systems,* 4th ed. Englewood Cliffs, NJ: Prentice-Hall, 2002.

[27] Evox-Rifa, 22.08.2007 RFI Capacitors for the AC Line (X and Y Capacitors), 2007.

[28] M. L. Heldwein, T. Nussbaumer, F. Beck, and J. W. Kolar, "Novel three-phase CM/DM conducted emissions separator," in *Proc. IEEE Appl. Power Electron. Conf. Expo.*, 2005, vol. 2, pp. 797–802.

Marcelo Lobo Heldwein (S'99–M'08) received the B.S. and M.S. degrees in electrical engineering from the Federal University of Santa Catarina, Florianópolis, Brazil, in 1997 and 1999, respectively, and the Ph.D. degree from the Swiss Federal Institute of Technology (ETH Zurich), Zurich, Switzerland, in 2007.

From 1999 to 2001, he was a Research Assistant in the Power Electronics Institute, Federal University of Santa Catarina. From 2001 to 2003, he was an Electrical Design Engineer with Emerson Energy Systems, São José dos Campos, Brazil, and Stockholm, Sweden. From 2008 to 2009, he was a Postdoctoral Fellow in the Power Electronics Institute (INEP), Federal University of Santa Catarina (UFSC), under the PRODOC/CAPES program. Since 2010, he has been an Adjunct Professor with the Electrical Engineering Department at the UFSC. His research interests include power-factor correction techniques, static power converters, and electromagnetic compatibility.

Dr. Heldwein is a member of the Brazilian Power Electronic Society (SOBRAEP).

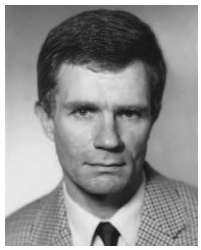

Hans Ertl (M'93) received the Dipl.-Ing. (M.Sc.) and the Dr.techn. (Ph.D.) degrees in industrial electronics from Vienna University of Technology, Vienna, Austria, in 1984 and 1991, respectively.

Since 1984, he has been with Vienna University of Technology, currently working as an Associate Professor of Power Electronics in the Institute of Electrical Drives and Machines. He has performed numerous industrial and scientific research projects in the areas of field-oriented control of ac drive systems, switch-mode power supplies for welding and industrial plasma processes, and active rectifier systems. He is the author or coauthor of numerous scientific papers and patents. His current research activities are focused on switch-mode power amplifiers and multicell topologies, in particular, for the generation of testing signals, for active ripple-current compensators, and for several applications in the area of renewable energy systems.

Juergen Biela (S'04–M'07) received the Diploma (with honors) in electrical engineering from Friedrich-Alexander University, Erlangen, Germany, in 2000, and the Ph.D. degree in electrical engineering from ETH Zurich, Zurich, Switzerland, in 2005. In the course of his M.Sc. studies, he dealt in particular with resonant dc-link inverters at the University of Strathclyde, Glasgow, U.K. (term project) and the active control of series-connected IGCTs at the Technical University of Munich (Diploma thesis).

He was with the Research Department, A&D Siemens, Germany, from 2000 to 2001, where he focused on inverters with very high switching frequencies, SiC components, and EMC. In July 2002, he joined the Power Electronic Systems Laboratory (PES), ETH Zurich, working toward the Ph.D. degree concentrating on optimized electromagnetically integrated resonant converters. From 2006 to 2007, he was a Postdoctoral Fellow in the PES and has been a Guest Researcher at the Tokyo Institute of Technology, Tokyo, Japan. Since 2007, he has been a Senior Research Associate in the PES. His current research interests include multidomain modeling, design and optimization of power electronic systems, in particular, systems for future energy distribution, and pulsed-power applications, advanced power-electronic systems based on novel semiconductor technologies, and integrated passive components for ultracompact and ultraefficient converter systems.

Johann W. Kolar (S'89–M'91–SM'04) received the Ph.D. degree (*summa cum laude*) in industrial electronics from the University of Technology Vienna, Vienna, Austria.

From 1984 to 2001, he was with the University of Technology Vienna, where he was teaching and working in research in close collaboration with industry in the fields of high-performance drives, high-frequency inverter systems for process technology, and uninterruptible power supplies. Since 2001, he has been a Professor and Head of the Power Electronic Systems Laboratory, Swiss Federal Institute of Technology Zürich, Zürich, Switzerland. The focus of his current research is on novel ac–ac and ac–dc converter topologies with low effects on the mains for telecommunication systems, More-Electric-Aircraft applications, and distributed power systems utilizing fuel cells. A further main area of research is the realization of ultracompact intelligent converter modules employing the latest power semiconductor technology (SiC) and novel concepts for cooling and electromagnetic interference filtering. He has authored or coauthored over 150 scientific papers in international journals and conference proceedings and has filed more than 50 patents.

Dr. Kolar is a member of the Institute of Electrical Engineers of Japan and of the Technical Program Committees of numerous international conferences (e.g., Director of the Power Quality branch of the International Conference on Power Conversion and Intelligent Motion). From 1997 to 2000, he served as an Associate Editor of the IEEE TRANSACTIONS ON INDUSTRIAL ELECTRONICS and, since 2001, as an Associate Editor of the IEEE TRANSACTIONS ON POWER ELECTRONICS.